Nanocomposites

DOI: 10.1002/anie.201104149

# Investigating the Amorphous–Crystalline Interplay in $SiO_2/TiO_2$ Nanocomposites by Total Scattering Methods**

*Giuseppe Cernuto, Simona Galli, Federica Trudu, Gian Maria Colonna, Norberto Masciocchi, Antonio Cervellino,* and Antonietta Guagliardi**

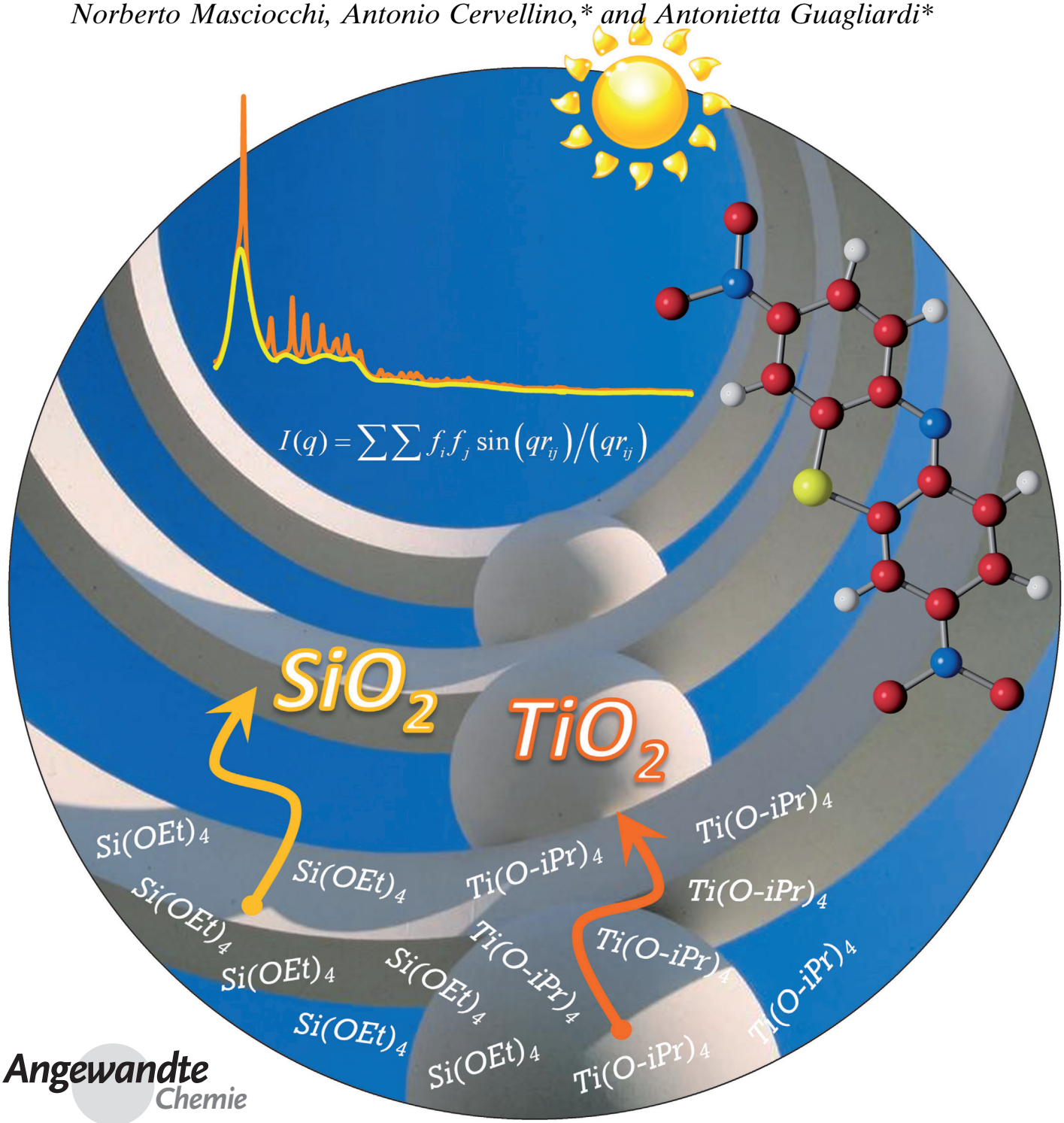

Hybrid materials offer the advantage of synergistically combining distinct properties of the individual components; accordingly, different combinations might be engineered to target desired performances or to explore possible novel properties of the composites.[1] One of the most appealing combinations is crystalline/amorphous hybrids. Among these materials, silica/titania nanocomposites[2] have been studied as systems that are able to combine the remarkable adsorption properties of amorphous porous silica and the excellent photocatalytic activity of crystalline titania nanoparticles.[3] $TiO_2$ is known to be one of the best-performing photocatalysts[4] among metal oxide semiconductors with important applications in environmental and energetic fields (wastewater pollution, water splitting, dye-sensitized solar cells, self-cleaning textiles). The possibility of overcoming the relatively low surface area of pure titania makes $SiO_2/TiO_2$ hybrids particularly suitable for air and water pollutant purification.[5] However, this kind of composites have been rarely characterized according to a unique and coherent approach, suitably addressed to quantitatively extract information on the mutual influence of each component under different synthetic conditions. Such a characterization would be extremely helpful in tailoring the synthesis and engineering of advanced systems, as long as it enables control of the composite properties over a gram scale. The latter requirement makes diffraction techniques, which are able to extract properties averaged over the irradiated volume, more suitable for structural investigations than the statistically limited microscopies, such as AFM, TEM, and HRTEM, commonly used in particles structure, interface, and morphology studies of pure and hybrid systems.

Structural details of amorphous materials are traditionally recovered by the total scattering pair/radial distribution function (PDF/RDF) technique[6] or by the Debye function (DF) method.[7] RDF is obtained by sine Fourier transforming the powder pattern, while DF uses the set of interatomic distances to model, in the reciprocal space, the experimental trace. Only recently, a DF-based method has been proposed[8] for nanosized anisotropic crystal domains, which is able to model both Bragg and diffuse scattering and, at the same time, to overcome the computational time limits of the Debye equation.[9] Compared to the more conventional Rietveld-based structural methods, which are only able to reproduce the Bragg scattering, and to the frequently used Scherrer equation (affording only average sizes), the new approach can provide information about the nanocrystal size and shape, as well as about their relative distributions on the basis of chemically sound models. The main aspects of our DF method are outlined in the Experimental Section; recent applications to $TiO_2$ nanoparticles can be found in ref. [10].

Herein we report on the (micro)structural characterization of sol–gel $SiO_2/TiO_2$ composites prepared at low temperature (80 °C) by tuning the content of the tetraethyl orthosilicate (TEOS) and titanium isopropoxide (TTIP) precursors (50:50, 65:35, and 80:20 Si/Ti molar ratios, labeled ST50, ST65, and ST80 in the following) and the ageing time (24, 48, and 120 h, marked as A, B, and C, respectively; see the Supporting Information).[11] All samples have been investigated by X-ray total scattering techniques using, for the first time, both reciprocal (DF) and real (RDF) space methods on the same experimental dataset, thus aiming at fully characterizing both the nanocrystalline and the amorphous fractions. Moreover, pure $SiO_2$ samples were prepared under the same temperature and ageing conditions (SA, SB, SC samples), and used as reference materials for the amorphous component.

$TiO_2$ photocatalytic efficiency is commonly related to the ability of synthesizing the most suitable polymorph (anatase, which is preferred to rutile and brookite), in high purity[12] and in small nanocrystals (NCs) of relatively high crystal perfection. Furthermore, a deep control of the crystal shape (aiming at developing the more active crystal facets)[13] and of the size and shape distributions is highly desirable. When embedded in an amorphous silica (a-$SiO_2$) matrix, the growth of pure anatase is favored[2a,14] and the formation of a core/shell structure (anatase/Ti–O–Si-modified titania),[15] as indicated by the blue-shift of the pure anatase absorption edge (from 3.20 to 3.54 eV) and the decrease of the crystal field at $TiO_2$–$SiO_2$ interface observed by XAS, is reported.[16]

In the present work, our combined DF/RDF approach was applied to the synchrotron X-ray powder diffraction data collected on the samples mentioned above, enabling us to: 1) quantitatively evaluate the amorphous matrix effects on the size and shape distributions of anatase NCs; 2) investigate the $TiO_2$–$SiO_2$ interface; and 3) understand how the $TiO_2$/$SiO_2$ interplay influences the electronic,[17] sorptive, and photocatalytic properties of the nanocomposites. Following the DF analysis described in the Experimental Section, we obtained the results given below and as graphical outputs in Figure 1–3. Satisfactory fits were reached for all samples (see the Supporting Information), in both nanocrystalline and amorphous components, regardless of their nominal relative fractions.

Figure 2 shows the collection of the 2D maps illustrating the bivariate size distribution of $TiO_2$ NCs. A strong correlation between the two growth directions (along the *c*-axis and in the orthogonal *ab*-plane) is found in all samples. Furthermore, a clear dependence of the size/shape distribution on both the composition and the ageing time is observed:

[*] Dr. G. Cernuto, Dr. S. Galli, Prof. N. Masciocchi
Dipartimento di Scienze Chimiche e Ambientali
Università dell'Insubria
via Valleggio 11, 22100 Como (Italy)
Dr. F. Trudu,[+] Dr. A. Guagliardi[+]
Istituto di Cristallografia, CNR
via Amendola 122/o, 70126 Bari (Italy)
E-mail: antonella.guagliardi@ic.cnr.it
Dr. G. M. Colonna
Stazione Sperimentale per la Seta
via Valleggio 3, 22100 Como (Italy)
Dr. A. Cervellino
Materials Science Beamline, SLS, Paul Scherrer Institut
Villigen (Switzerland)
E-mail: antonio.cervellino@psi.ch
[+] Present address: Università dell'Insubria (Italy)
[**] Partial support by Fondazione Cariplo, Project 2009-2446. Diffraction data of all samples were recorded at the MS4 Powder beamline of the SLS synchrotron, Villigen, CH.
Supporting information for this article is available on the WWW under http://dx.doi.org/10.1002/anie.201104149.

  

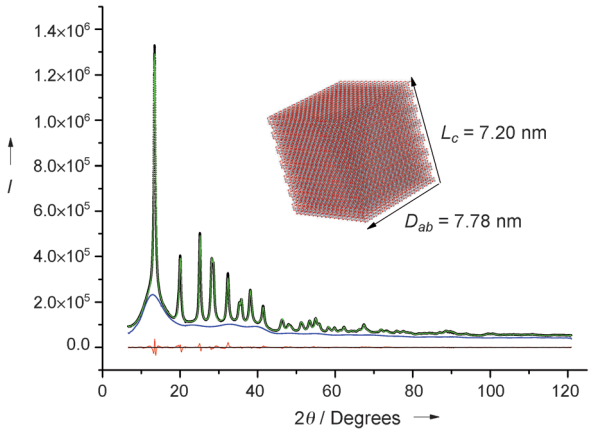


***Figure 1.*** Best fit obtained by the DF analysis on the ST50C sample. Experimental data as black dots; total calculated trace as solid green line with the amorphous trace highlighted under the peaks; difference line (Exp-Calc) at the bottom. The anatase NC model corresponding to the average size and shape computed from the experimentally derived size/shape distributions is shown in the insert.

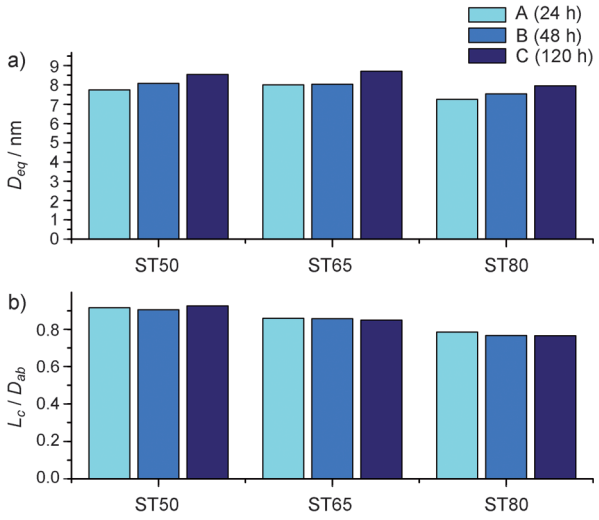


***Figure 3.*** a) Average size, $D_{eq}$, and b) aspect ratio, $L_c/D_{ab}$, of anatase NCs. Note that, since the size distributions are significantly asymmetric, the mean values (7 to 9 nm) do not coincide with the distribution maxima (falling near 5 nm in Figure 2).

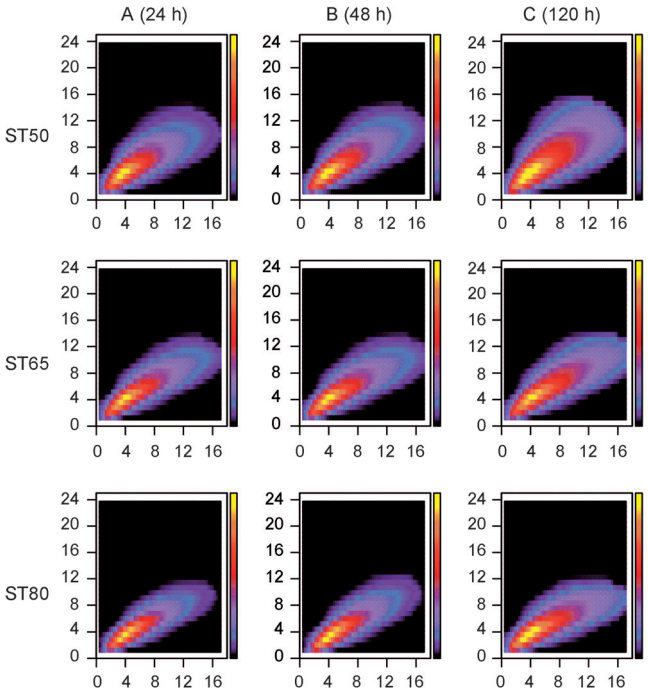


***Figure 2.*** Collection of the bivariate size distribution maps of anatase NCs provided by the DF analysis. Horizontal axis: diameter of the equivalent circle in the *ab*-plane. Vertical axis: crystal size along the *c*-axis (values in nm).

the distribution becomes wider upon ageing, whereas an opposite effect is observed upon increasing the amorphous fraction. Accordingly, the two effects appear most pronounced in the two extreme cases: ST50C and ST80A.

Average NC sizes and aspect ratios, derived from the distributions shown above, are synoptically collected in Figure 3. Small sizes are found (with $D_{eq}$ values—the diameter of the sphere of equivalent volume—below 9 nm), along with aspect ratios $L_c/D_{ab}$ always below 1 ($L_c$ is the average crystal size along the *c*-axis and $D_{ab}$ is the diameter of the circle of equivalent area, in the *ab*-plane). Weak, but detectable, systematic effects on both size and shape are evaluated: smaller average sizes are formed at low ageing times and at larger silica fractions. Similarly, a progressively more anisotropic shape is favored for larger amorphous content, down to an average aspect ratio of 0.77 (ST80).

Interestingly, the calculated diffraction traces of the amorphous component (provided by the DF analysis as separate signals) did not exactly match the corresponding experimental patterns of pure $SiO_2$ (see Figure 4a), prompting us to investigate the short-range order of the amorphous matrices by the (complementary) RDF method. The main results, given as $G(r)$, are shown in Figure 4b (C samples); similar findings are obtained for the other samples (see the Supporting Information).

Besides the expected Si–O and Si–Si interatomic distances (1.5 Å and 3.0 Å, respectively), new features clearly emerge in the ST50 sample, and are weakly perceptible in the others (more $TiO_2$-diluted). In particular, a weak shoulder at 2.0 Å and a more pronounced one at 3.7 Å are present, corresponding to the Ti–O and Ti–Ti distances in corner-sharing octahedra, respectively, thus giving evidence of the presence of amorphous titania (a-$TiO_2$). The Si–Ti distance (ca. 3.2 Å), witnessing the occurrence of a Ti–O–Si link between $TiO_6$ octahedra and $SiO_4$ tetrahedra, could not be clearly assessed by RDF, because of the occurrence of multiple (Si–Si and Ti–Ti in edge-sharing octahedra) distances overlapping around 3.0–3.2 Å, but was confirmed by IR spectroscopy[18] (see the Supporting Information).

We also estimated the $TiO_2$ fraction in the amorphous matrix by coupling the (DF-derived) integral areas under the crystalline and amorphous traces. The weight fractions of anatase, a-$TiO_2$, and a-$SiO_2$ are given in Figure 5 for all the composites. A significant percentage (about 16, 14, and 10%

  

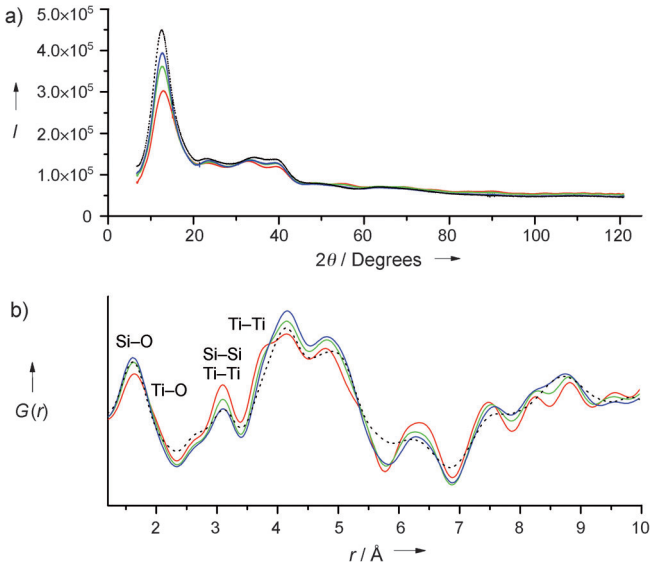


***Figure 4.*** a) Amorphous traces derived from the DF analysis; b) $G(r)$ (the probability of finding two atoms at the distance r, weighted by atomic numbers) of the patterns shown in (a). Colour codes: ST50C (red), ST65C (green), and ST80C (blue) [bottom to top in (a)]. The experimental diffraction pattern and the RDF trace of pure $SiO_2$ (SC, dashed line) are included for comparison.

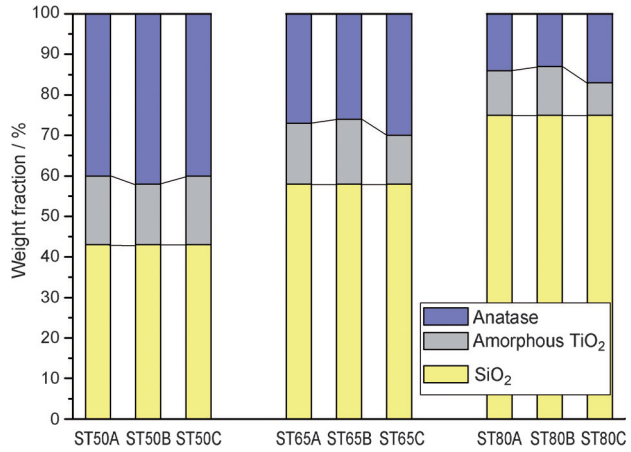


***Figure 5.*** Crystalline (anatase) and amorphous ($TiO_2$ and $SiO_2$), weight fractions (%) estimated for the investigated samples. Nominal fractions of total $TiO_2$ are 57% (ST50), 42% (ST65), and 25% (ST80).

of the total weight in the ST50, ST65, and ST80 samples, respectively) turned out to be a-$TiO_2$, with small fluctuations depending on ageing (or on the accuracy of the method). To shed light on the location of the a-$TiO_2$ in the composites, we performed the DF analysis on a calcined sample (ST50C heated in air at 550 °C). Its $D_{eq}$ increases from 8.5 to 10.8 nm and, surprisingly, also the morphology of the NCs changes to a lower $L_c/D_{ab}$ (from 0.93 to 0.80). These findings suggest the existence of a non-uniformly distributed a-$TiO_2$ shell, reasonably located at the interface between anatase NCs and silica matrix, rather than of significant amounts of a-$TiO_2$ islands dissolved in a-$SiO_2$.

The derived nanocomposite properties were compared to independent estimates of the porosity, adsorption, photocatalytic efficiency and UV-Vis light absorption. To this aim, specific surface areas (SSA, BET model), the variation of the concentration of methylene blue (MB) solutions when the powders were suspended in the dark (adsorption) and upon light exposure, and energy band gaps ($E_g$) were derived (see the Supporting Information). SSA of composites increases with the amorphous fraction (in the 450–670 $m^2 g^{-1}$ range) for all ageing times (see Figure 6a), with the value for ST80A, surprisingly, being larger than that of the corresponding pure silica sample SA.

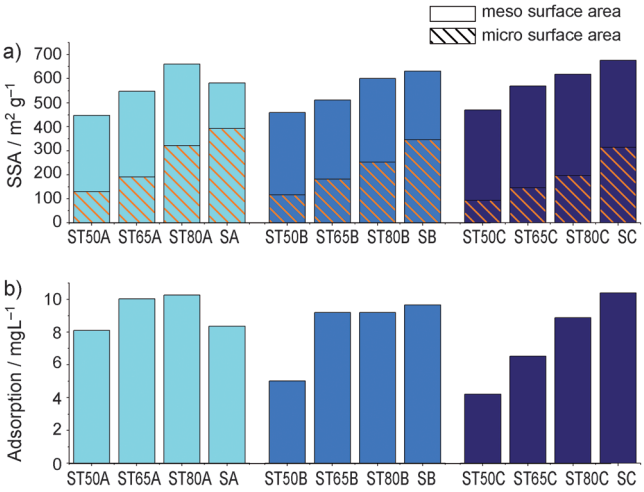


***Figure 6.*** a) SSA values and b) relative amount of adsorbed MB in nanocomposites and pure silica samples.

In all samples, systematically larger surfaces, due to microporosity, are observed on increasing the a-$SiO_2$ content, resulting in a variety of micro- and meso-pore distributions, which seems to strongly control the adsorption of MB molecules (see Figure 6b). At variance, smaller surfaces occur for prolonged ageing. The most favorable combination, leading to larger SSA values, seems to occur for aged silica samples (SB and SC) and by the joint action of mild ageing and limited $TiO_2$ fraction in the ST80A composite (micro/mesopores SSA ratios: 0.55, 0.47, and 0.48, respectively).

The photocatalytic activity of $TiO_2$ NCs is given in Figure 7 for all the composites. Taking into account the results summarized in Figure 3, a clear inverse dependence of the apparent kinetic constant with the size of the NCs (for equal $TiO_2$ content) and with the aspect ratios (across different $TiO_2$ compositions) is observed. The best combination is found, again, in the ST80A sample, the composite also having the best adsorption properties.

Finally, the $E_g$ values fall in the 3.08–3.22 eV range; the small, systematic red-shift is registered for the higher $TiO_2$ content (ST50 and ST65 samples); no significant changes are observed upon ageing. To the best of our knowledge, two possible reasons for this behavior may be invoked: 1) the presence of a-$TiO_2$ (known to reduce the $E_g$ values[19]), and 2) the occurrence of surface defects (Ti sof, estimated by DF

  

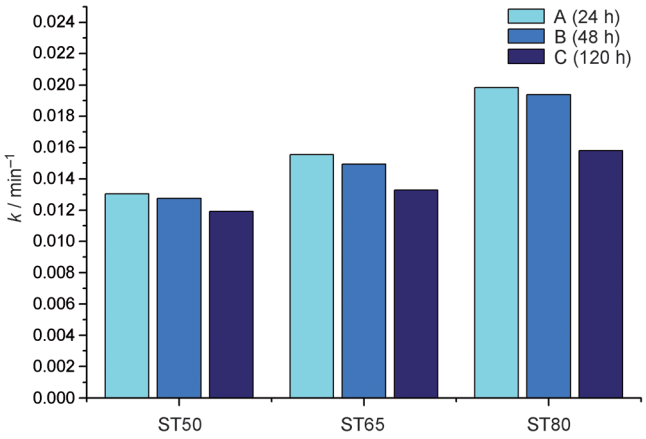


***Figure 7.*** Apparent kinetic constants ($k$, $min^{-1}$, in the pseudo-first-order approximation) for MB discoloration promoted by anatase in $TiO_2/SiO_2$ nanocomposites.

analysis—see the Supporting Information—fall in the 0.87–0.90 range). An opposite effect was found by Li and Kim[16a] on similar composites prepared by a different route and calcined at 480 °C. However, we measured an $E_g$ of 3.19 eV also in our calcined sample.

In summary, a combined DF/RDF total scattering approach has been used, for the first time, to give a coherent picture of the amorphous/crystalline interplay in silica/titania hybrid materials as a function of samples composition and ageing. The ability to quantitatively address by this new method a number of structural and microstructural features in anisotropically shaped crystal domains and amorphous fractions, thus increasing the structural chemist's toolbox, has proved to be a useful tool in interpreting subtle functional property modifications and for designing better-performing materials. It is worth noting that highly valuable spectroscopic techniques (solid-state NMR and IR) are currently used in characterizing similar hybrid nanocomposites, but with limited chances of discriminating the amorphous or nanocrystalline origin of the signals.

## Experimental Section

Synthesis: Silica/titania nanocomposites were prepared using a sol–gel synthetic procedure, by adding (dropwise under stirring) a mixture of tetraethyl orthosilicate (TEOS) and titanium tetraisopropoxide (TTIP) with the desired Si/Ti molar ratio (50:50, 65:35, and 80:20), to a 1.4 M HCl solution in water and ethanol [(TEOS + TTIP)/$H_2O_{HCl\,1.4\,M}$/EtOH molar ratio 1:25:15]. Hydrolysis was obtained leaving the sols under stirring for 24 h at RT; the gels of each composition were then separated into three portions and aged in closed bottles at 80 °C for 24, 48, and 120 h, resulting in nine different samples that were finally dried at RT. Pure silica samples (SA, SB, and SC) were prepared using TEOS only and used as reference materials for the nanocomposite amorphous fractions.

X-ray characterization: Diffraction data were collected at the Materials Science beamline of the Swiss Light Source synchrotron facility at the Paul Scherrer Institute, from samples loaded in 0.5 mm glass capillaries, using a Debye–Scherrer geometry and approximately 15 keV radiation ($\lambda = 0.827006$ Å), partial He beam path, and a Mythen detector covering 115° with 0.0038° resolution. Data were carefully subtracted for absorption-corrected air and capillary scattering contributions before DF analysis.

The DF method used for the characterization[10] of anatase NCs relies on: 1) the generation of a bivariate population of $D_{4h}$ prismatic crystals of variable shape and size (platelets to rods); 2) the calculation, for each NC, of a set of sampled interatomic distances (instead of the true ones), later stored in a suitable database; 3) the use of a modified and fast Debye equation algorithm. The entire process allows to reduce the number of distances involved in the Debye equation by orders of magnitude, thus making it possible to obtain pattern simulations the accuracy of which is within 1 ppm of the ideal pattern and to speed up the use of iterative global optimization algorithms while refining several model parameters. In the present work, the sampled distances database used for pattern simulations included 1000 NCs with a maximum size up to 15 nm in the *ab*-plane and 24 nm along the *c*-axis. The experimental diffraction patterns of pure $SiO_2$ samples were used as an initial estimate of the amorphous component and 50 additional Chebyshev polynomial coefficients were necessary to reproduce a satisfactory (and wavy) amorphous trace. A Simplex algorithm[20] was employed to explore the parameter space (averages and standard deviations of the bivariate log-normal size distribution - one pair for each growth direction - and their correlation angle; Ti occupancy factors and three coefficients modeling the possible size-dependence of the atomic Debye-Waller factors) and to reach a reliable fit for each sample.

Physical characterization: Details of measurements of $N_2$ absorption/desorption isotherms, photocatalytic activity, IR, and diffuse reflectance spectra can be found in the Supporting Information.

Received: June 16, 2011
Published online: September 12, 2011

**Keywords:** nanocomposites · nanotechnology · structure–property relationships · X-ray diffraction

[1] a) *Hybrid Nanocomposites for Nanotechnology: Electronic, Optical, Magnetic and Biomedical Applications* (Ed.: L. Merhrari), Springer, New York, **2009**; b) R. Costi, A. E. Saunders, U. Banin, *Angew. Chem.* **2010**, *122*, 4996 – 5016; *Angew. Chem. Int. Ed.* **2010**, *49*, 4878 – 4897.
[2] a) R. J. Davis, Z. Liu, *Chem. Mater.* **1997**, *9*, 2311 – 2324; b) V. Zeleňák, V. Hornebecq, S. Mornet, O. Schäf, P. Llewellyn, *Chem. Mater.* **2006**, *18*, 3184 – 3191.
[3] C. Anderson, A. J. Bard, *J. Phys. Chem.* **1995**, *99*, 9882 – 9885.
[4] a) X. Chen, S. S. Mao, *Chem. Rev.* **2007**, *107*, 2891 – 2959; b) D. A. H. Hanaor, C. C. Sorrell, *J. Mater. Sci.* **2011**, *46*, 855 – 874.
[5] a) K. Y. Jung, S. B. Park, *Appl. Catal. B* **2000**, *25*, 249 – 256; b) K. Qi, X. Chen, Y. Liu, J. H. Xin, C. L. Mak, W. A. Daoud, *J. Mater. Chem.* **2007**, *17*, 3504 – 3508; c) E. Pitoniak, C.-Y. Wu, D. W. Mazyck, K. W. Powers, W. Sigmund, *Environ. Sci. Technol.* **2005**, *39*, 1269 – 1274; d) H. R. Jafry, M. V. Liga, Q. Li, A. R. Barron, *Environ. Sci. Technol.* **2011**, *45*, 1563 – 1568.
[6] a) *Underneath the Bragg Peaks*: *Structural Analysis of Complex Materials* (Eds.: T. Egami, S. J. L. Billinge), Elsevier, Amsterdam, **2003**; b) P. Scherrer, *Nachr. K. Ges. Wiss. Goettingen Math.-Phys. Kl.* **1918**, *2*, 98.
[7] P. Debye, *Ann. Phys.* **1915**, *46*, 809 – 823.
[8] A. Cervellino, C. Giannini, A. Guagliardi, *J. Appl. Crystallogr.* **2010**, *43*, 1453 – 1457; A. Cervellino, A. Guagliardi in *Diffraction at the Nanoscale: Nanocrystals, Defective and Amorphous Materials* (Eds.: N. Masciocchi, A. Guagliardi), Insubria University Press, Varese, **2010**, pp. 107 – 126.
[9] A. Cervellino, C. Giannini, A. Guagliardi, *J. Comput. Chem.* **2006**, *27*, 995 – 1008.

  

[10] G. Cernuto, N. Masciocchi, A. Cervellino, G. M. Colonna, A. Guagliardi, *J. Am. Chem. Soc.* **2011**, *133*, 3114 – 3119.
[11] Our nanocomposites highly differ from the silica-coated P25 nanoparticles reported in ref. [5d], which, not being prepared by an in situ process, retain, after silica addition, the original features of the pristine material.
[12] a) H. Zhang, M. Finnegan, J. F. Banfield, *Nano Lett.* **2001**, *1*, 81 – 85; b) C. Wang, J. Y. Ying, *Chem. Mater.* **1999**, *11*, 3113 – 3120; c) K. Yanagisawa, J. Ovenstone, *J. Phys. Chem. B* **1999**, *103*, 7781 – 7787.
[13] a) J. Pan, G. Liu, G. Q. Lu, H. Cheng, *Angew. Chem.* **2011**, *123*, 2181 – 2185; *Angew. Chem. Int. Ed.* **2011**, *50*, 2133 – 2137; b) A. S. Barnard, P. Zapol, *J. Phys. Chem. B* **2004**, *108*, 18435 – 18440.
[14] M. Hirano, K. Ota, H. Iwata, *Chem. Mater.* **2004**, *16*, 3725 – 3732.
[15] J. P. Espinós, G. Lassaletta, A. Caballero, A. Fernández, A. R. González-Elipe, A. Stampfl, C. Morant, J. M. Sanz, *Langmuir* **1998**, *14*, 4908 – 4914.
[16] a) Y. Li, S.-J. Kim, *J. Phys. Chem. B* **2005**, *109*, 12309 – 12315; b) L. Soriano, G. G. Fuentes, C. Quirós, J. F. Trigo, J. M. Sanz, P. R. Bressler, *Langmuir* **2000**, *16*, 7066 – 7069.
[17] V. Luca, *J. Phys. Chem. C* **2009**, *113*, 6367 – 6380.
[18] Z. Ding, G. Q. Lu, P. F. Greenfield, *J. Phys. Chem. B* **2000**, *104*, 4815 – 4820, and references therein.
[19] A. Langereis, S. D. S. Heil, H. C. M. Knoops, W. Keuning, M. C. M. van de Sande, W. M. M. Kessels, *J. Phys. D* **2009**, *42*, 073001.
[20] J. A. Nelder, R. Mead, *Comput. J.* **1965**, *27*, 308 – 316.

  